

Band engineering of ternary metal nitride system $Ti_{1-x}Zr_xN$ for plasmonic applications

Mukesh Kumar,^{1,2,*} Satoshi Ishii,^{2,3} Naoto Umezawa,^{1,2} and Tadaaki Nagao^{2,3}

¹Environmental Remediation Materials Unit, National Institute for Materials Science, Ibaraki 305-0044, Japan

²CREST, Japan Science and Technology Agency, 4-1-8 Honcho, Kawaguchi, Saitama, 332-0012, Japan

³International Center for Materials Nanoarchitectonics (MANA), National Institute for Materials Science (NIMS), Tsukuba 305-0044, Japan

*mkgarg79@gmail.com, Kumar.Mukesh@nims.go.jp

Abstract: Chemical composition is the primary factor that determines the electronic band structure and thus also influences the optical properties of plasmonic ceramics including nitrides and oxides. In this work, the optical and plasmonic properties of TiN, ZrN and their hypothetical intermediate alloys $Ti_{1-x}Zr_xN$ ($x = 0, 0.25, 0.50, 0.75, \text{ and } 1$), are studied by using first-principles density functional theory. We demonstrate the effects of electronic band structure tuning (band engineering) on the dielectric properties by varying the concentration of metallic constituents. Our calculations reveal that bulk plasma frequency, onset of interband transitions, width of bulk plasmon resonance and cross-over frequency, can be tuned flexibly in visible spectrum region by varying the amount of Zr concentration in $Ti_{1-x}Zr_xN$ alloy system. We found that low threshold interband energy onset (~ 1.95 eV) leads to high losses in Ti rich compounds than that of ZrN which points to lower losses.

1. Introduction

Plasmonics has opened the door for many technological applications such as bio-sensing [1], solar energy harvesting [2], plasmonic circuit [3] to name but a few in the past decade. Gold (Au) and silver (Ag) have been commonly used in these applications due to their large plasma frequencies and low losses (small plasmon damping). However, noble metals are too expensive for mass productions and the magnitudes of the real parts are too large, which is not suitable for fabricating metamaterials and transformation optics devices for practical uses [4]. Also the mechanical strength, as well as stability at high temperature are lacking in these noble metal elements. Because of these reasons, studies on alternative plasmonic materials such as intermetallics, metal alloys, transparent conductive oxides, and refractory compounds, have been on high demands in the past few years [5-10]. In this context, transition metal nitrides such as titanium nitride (TiN) and zirconium nitride (ZrN) were proposed for plasmonic applications in the visible frequencies range as alternative plasmonic materials [11-14]. Obviously they are much more inexpensive than noble metals and the real parts of permittivities are negative with reasonably large magnitudes. In addition, properties like high melting point temperature, chemical stability, and resistivity against abrasion, make them promising for the use in plasmonic applications in harsh environment [11-16]. Moreover, due to their simple cubic lattice structures, these materials can be grown epitaxially on various substrates like Si, MgO and crystalline sapphire [6]. There are many reports where optical properties of TiN and ZrN for plasmonic application have been discussed [12-16], however, to the best of our knowledge not a single study is reported on alloy composition of $Ti_{1-x}Zr_xN$ nor the tunability of their optical properties. With this regard, theoretical approach based on first-principles density functional theory (DFT), is quite powerful in the study of electronic and optical properties of materials due to its superiority in control. Therefore, present study is designed accordingly and the electronic and optical properties of $Ti_{1-x}Zr_xN$ ($x = 0, 0.25, 0.50, 0.75 \text{ and } 1$) alloy system are studied within theoretical domain by using both DFT and electromagnetic (or Mie theory) simulations. Our study reveals that optical properties of hypothetical ternary nitride alloys $Ti_{1-x}Zr_xN$, vary smoothly between those of TiN and ZrN. With the help of band engineering, the optical parameters including cross-over frequency, bulk plasmon energy, and interband transitions can be tuned to required frequencies in the visible spectrum for desired plasmonic applications. Details are discussed in this article.

2. Model, Methods and Computational details

Electronic band structure, optical and plasmonic properties of materials can be obtained easily from number of various methods like time-dependent DFT, many-body perturbation theory and independent particle approximation (IPA) with appropriate relativistic correction [17-24]. Here, we apply IPA, a successful approach used previously to examine the dielectric function of many metallic systems [19, 23, 24]. The dielectric function of metals have contribution from both intraband (intra) and interband (inter) electron transitions. Hence, the total dielectric function is the sum of both intra and inter terms,

$$\varepsilon(\omega) = \varepsilon_{\text{intra}}(\omega) + \varepsilon_{\text{inter}}(\omega) \quad (1)$$

The intra part, $\varepsilon_{\text{intra}}(\omega)$ of dielectric function was obtained from simple Drude model scheme [25],

$$\varepsilon_{\text{intra}}(\omega) = \mathbf{1} - \frac{\omega_p^2}{\omega(\omega + i\gamma)} \quad (2)$$

where ω_p and γ are the plasma frequency and damping parameter due to the dispersion of the electrons, respectively. One can obtain ω_p from electronic band structure as discussed elsewhere [23], whereas γ can be either obtained from experimental data or from higher order calculation [25]. The inter part of dielectric function $\varepsilon_{\text{inter}}(\omega) = \varepsilon_1(\omega) + i\varepsilon_2(\omega)$ (where ε_1 is the real part and ε_2 is the imaginary part) was obtained from electronic band structure calculation. First, imaginary part was calculated by evaluating direct electronic transition between occupied and unoccupied electronic states and then real part was obtained from the Kramers-Kronig transformation as per method discussed elsewhere [26] and also in our previous studies [27, 28], where the dielectric function of various semiconductors were calculated.

Once dielectric function is evaluated, the electron loss function $ELF(\omega)$ and reflectivity $R(\omega)$ were evaluated from the following formulations, [25]

$$ELF(\omega) = \mathbf{Im}\left(-\frac{1}{\varepsilon(\omega)}\right) \quad (3)$$

$$R(\omega) = \left| \frac{(1 - \sqrt{\varepsilon(\omega)})^2}{(1 + \sqrt{\varepsilon(\omega)})} \right|^2 \quad (4)$$

All these calculations of $\text{Ti}_{1-x}\text{Zr}_x\text{N}$ alloy system were performed using DFT as implemented in Vienna ab initio Simulation Package code [29]. Projector augmented wave-function type pseudo-potentials along with generalized gradient approximation of Perdew-Burke-Ernzerhof (PBE) [30] was used for the exchange-correlation potential. A Brillouin integration grid was built using the Monkhorst-pack scheme with $21 \times 21 \times 21$ and $29 \times 29 \times 29$ points for electronic band structure and optical permittivity calculation, respectively. The rocksalt structure (Fm-3m: space group No. 225) of TiN and ZrN was considered for calculations in this study. It is reported that 8 atoms cells can describe various alloy compositions efficiently for alloy structure like $\text{Au}_x\text{Pt}_{1-x}\text{Al}_2$ and the effect of disordered filling of cation metal sites on optical properties is relatively subtle [31]. Therefore, in present study, a cell of 8 atoms was used throughout the calculation to keep the discussion of alloy system $\text{Ti}_{1-x}\text{Zr}_x\text{N}$ in line with TiN and ZrN system. Only ordered alloy compounds are simulated here as calculations require a periodic structure. Among various available configurations for cation alloying, the most energetically stable configuration was considered for alloying. Figures 1(a) and 1(b) show the crystal structure of primitive and 8 atoms cell of TiN compound, while Fig. 1(c) represents the $\text{Ti}_{0.5}\text{Zr}_{0.5}\text{N}$ alloy configuration.

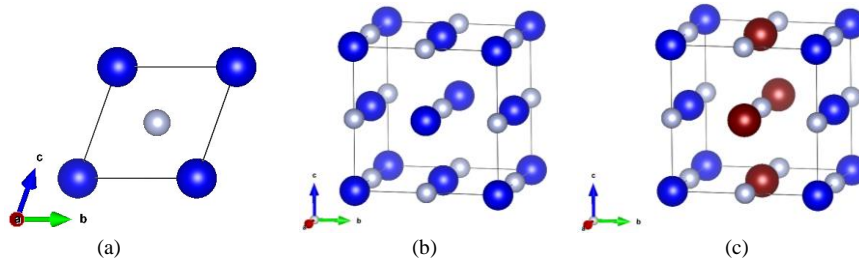


Fig.1 Crystal structure of the ordered alloy compounds (a) 2 atoms primitive cell of TiN, (b) 8 atoms cell of TiN and (c) 8 atoms cell of $\text{Ti}_{0.5}\text{Zr}_{0.5}\text{N}$ alloy. Here small balls represent N atom, whereas big blue and red ball represent Ti and Zr atoms, respectively.

3. Results

In this section we discuss the electronic and optical properties of $\text{Ti}_{1-x}\text{Zr}_x\text{N}$ alloy system. The calculated lattice parameters (TiN: 4.239 Å; $\text{Ti}_{0.75}\text{Zr}_{0.25}\text{N}$: 4.332 Å; $\text{Ti}_{0.5}\text{Zr}_{0.5}\text{N}$: 4.433 Å; $\text{Ti}_{0.25}\text{Zr}_{0.75}\text{N}$: 4.510 Å; and ZrN: 4.578 Å), are in good agreement with reported experimental values [32]. The linear increase in volume with Zr alloying shows the isostructural feature of these alloys.

3.1 Electronic Properties

Figures 2(a) and 2(b) show the calculated electronic band structure of base compounds TiN and ZrN respectively. Our calculated band structure of TiN and ZrN are consistent with earlier calculation [24].

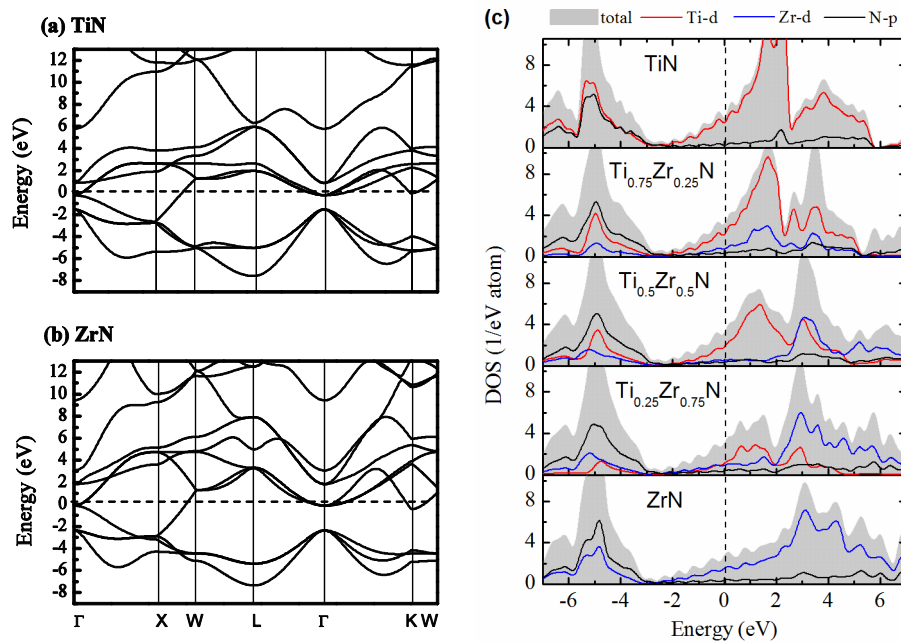


Fig.2 Calculated electronic band structure of (a) TiN, (b) ZrN along high symmetry directions and (c) DOS of $\text{Ti}_{1-x}\text{Zr}_x\text{N}$ alloy compounds. The dotted horizontal and vertical lines indicate the Fermi-level in left and right side panels, respectively.

One can clearly see that the bands cross the Fermi-level (E_f) (dotted horizontal lines) and hence no energy gap, confirms the metallic behavior of these materials. With the increase of lattice parameters from TiN \rightarrow ZrN, the Fermi-level shifted upwards from the valence band (VB) region to the conduction band (CB) region. This can be attributed to the bonding/antibonding split off phenomena, as Ti d states are lower in energy than Zr d states. The basic difference comes from the band at Γ -point. This can be understood from the density of states (DOS) plots of these compounds. Figure 2(c) shows the DOS of $Ti_{1-x}Zr_xN$ alloy system. One can see that partially filled d bands are located near the E_f . Since selection rule forbids the $d-d$ transitions, the only allowed optical transitions from $p \rightarrow d$, which is from hybridized N p and Ti/Zr d orbits along the Γ point of the 1st Brillouin zone. It is worth to mention that the position of the p band with respect to the E_f is lower in ZrN than in TiN by around 0.5 eV. This indicates that a higher energy is required for the interband $p \rightarrow d$ transitions to occur in ZrN. Based on the position of the band edge energies at the Γ point, one can estimate the threshold energy of the interband transitions which is related to the optical loss in materials. Our electronic structure calculations show that TiN has lower threshold energy (~ 1.9 eV), whereas ZrN has higher threshold energy (~ 2.6 eV). Hence, in the low energy region, it is expected that TiN has more optical losses than ZrN, whereas the alloy system lies between them.

3.2 Optical Properties

Before discussing the alloy composition, we calculate the optical properties of Au, a bench mark material in plasmonic field, by using the same simulation scheme as described above. The calculated optical properties (shown in Table 1) shows that the predicted optical properties are in reasonable agreement with reported experimental results. Figure 3(a) and 3(b) show the calculated imaginary (optical losses) and real permittivity, respectively in Au along with the individual contribution from intraband and interband transitions. For comparison we also show the latest experiment data of single crystal Au sample [33] in the available range from 0.05 – 4.14 eV.

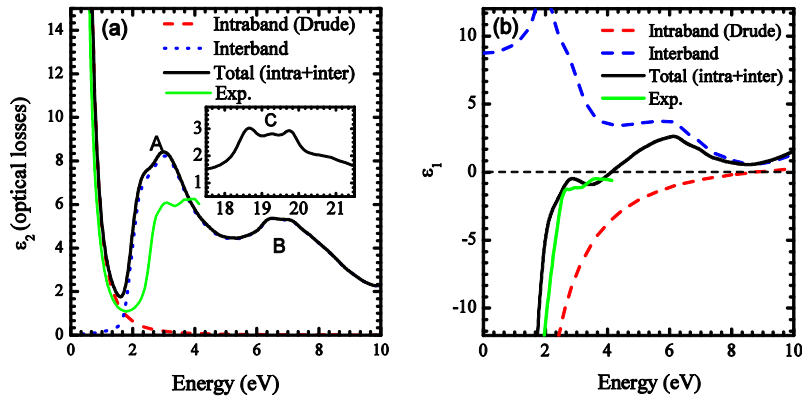


Fig.3 Calculated (a) Imaginary (optical losses) and (b) real permittivity in Au along with the individual contribution from intraband and interband transitions. Inset in Fig (a), shows the imaginary part at higher energy scale to observe other relevant peaks. Green solid line shows the experimental data for comparison.

Here in Fig. 3(a), we present the optical spectra in the energy range up to 10 eV (see inset for high energy scale). One can see the interband onset at ~ 1.8 eV followed by other major peaks at 3 eV and 7 eV. Apart from this, there are some more peaks at high energy scale $\sim 19-20$ eV as shown in the inset of Fig 3(a) (indicated as C point). Our presented spectra agree well with the reported calculations for the energy range 0-25 eV [19]. One can interpret the losses shown in Fig. 3 (a) from interband and intraband contribution. The interband losses in Au are high above 1.8 eV, on the other hand, intraband losses are negligible above 2 eV and very high in low energy (NIR) region. Overall, the essential features in the permittivity of Au are captured well in our work and consistent with experiments [33] and theory [19], which confirms the reliability of adopted methodology.

Figures 4(a) and 4(b) show the calculated real and imaginary parts of dielectric functions of $\text{Ti}_{1-x}\text{Zr}_x\text{N}$ alloy system. It is noticeable that TiN shows more loss compared to ZrN and this loss decreases with Zr alloying in $\text{Ti}_{1-x}\text{Zr}_x\text{N}$ alloy. The optical losses in these compounds can be correlated to the electronic structure. The position of p states are different for TiN and ZrN (c.f. Fig. 2), which generally influence the ω_{int} or optical loss. For example in the case of TiN, N p states are below ~ 1.9 eV from E_f whereas for ZrN, these states are well below 2.6 eV from E_f . As discussed in the previous section, this is the reason that the threshold energy for interband transitions is 1.9 eV for TiN and 2.6 eV for ZrN. The calculated optical parameters such as plasma frequency (ω_p), cross-over frequency (ω_c : corresponding value when $\epsilon_1(\omega)$ crosses zero), width of plasmon (WP: corresponding value of $\epsilon_2(\omega)$ when $\epsilon_1(\omega) = 0$), and onset of interband transitions (ω_{int}) are shown in Table 1, which are in good agreement with the reported experimental data for TiN and ZrN [34-37]. In addition, our calculated ω_p value of 7.49 eV for TiN and 8.63 eV for ZrN, are in good agreement with the previously reported DFT values of 7.62 eV and 8.82 eV for TiN and ZrN, respectively [24].

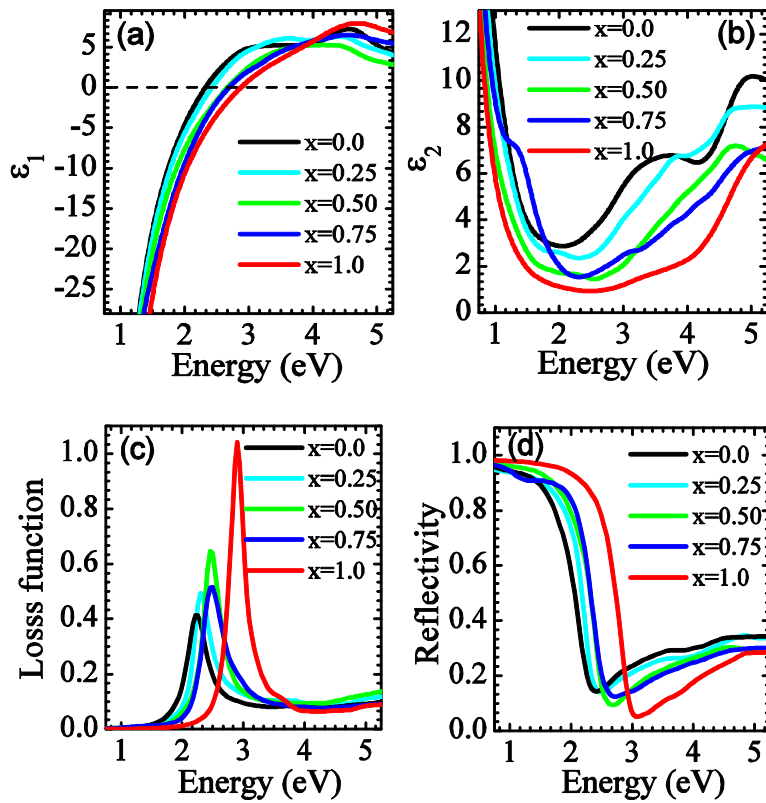


Fig.4 Calculated (a) real permittivity, (b) imaginary permittivity, (c) loss function, and (d) normal incident reflectivity of $\text{Ti}_{1-x}\text{Zr}_x\text{N}$ ($x = 0, 0.25, 0.5, 0.75$ and 1) alloy system.

Figure 4(c) shows the calculated frequency dependent energy loss function of $\text{Ti}_{1-x}\text{Zr}_x\text{N}$ alloy. The loss function has peaks (ELS_{peak}) at the frequencies where the real part of dielectric function becomes zero. Therefore one can verify the ω_c with these peak maxima of energy loss function. Estimated energies of the low-energy ELS_{peak} of bulk plasmons from loss function are depicted in Table 1. The peak for TiN is at 2.4 eV and a blue shift in peaks are observed for $\text{Ti}_{1-x}\text{Zr}_x\text{N}$ with increasing Zr concentration. Calculated low-energy plasma excitation of TiN at 2.4 eV and ZrN at 3.3 eV, are in reasonable agreement with measured peak at 2.8 eV [36] and 3.6 eV [37], respectively. However, one should note that local-field effect, spin-orbit coupling effect and quasi particle (GW) effect may lead to minor deviations of ± 0.5 eV in reported values, which however was not considered here.

Figure 4(d) shows the calculated reflectivity of alloy system at normal incident. Qualitatively, one can estimate the appearance of these materials in bulk based on the calculated reflectivity. Larger reflectivity (>60%) suggests the metallic like surface for these alloys in low wavelength region. TiN shows large reflectivity than ZrN. However, at longer wavelength, the trend is opposite and ZrN shows larger reflectivity than TiN. Note that a reflectivity edge is correlated to the cross-over frequency. Our analysis shows that the bulk plasmon energy of $Ti_{1-x}Zr_xN$ alloy falls in the range of visible wavelength and one can tune this energy by varying Ti/Zr concentration accordingly in the range of 2.3 to 2.9 eV (430 to 540 nm in wavelength).

Overall, one can summarize that the position of E_f , nitrogen p states and band edge energies at Γ point influence the optical loss in low energy region for these materials and there is basically monotonic shifts. As a result, one can tune the properties of the alloy system by varying Ti or Zr composition. For example it is possible to have a material having arbitrary ω_c between 2.32 eV and 2.86 eV by tuning the alloy composition. Monotonic changes in the optical properties indicate that the extreme cases are found either at $x = 0$ (TiN) or $x = 1$ (ZrN). Due to the low onset of the interband transitions, TiN have highest loss in low frequency region of the visible spectrum and can be used for applications in broadband light absorption as discussed in the next section. In contrast, ZrN has the lowest loss and can be a good choice for plasmonic waveguides and sensing applications.

Table 1. Calculated optical parameters, plasma frequency (ω_p), cross-over frequency (ω_c), width of plasmon (WP), onset of interband transitions (ω_{int}), and low-energy bulk plasmon peak (ELS_{peak}) of $Ti_{1-x}Zr_xN$ alloy system along with Au for comparison.

Material	ω_p (eV)	ω_c (eV)	WP (eV)	ω_{int} (eV)	ELS _{peak} (eV)
TiN	7.49 (6.69-8.7) ^{a,b}	2.32	3.12	1.95	2.38 (2.8) ^c
$Ti_{0.75}Zr_{0.25}N$	7.48	2.43	2.41		2.41
$Ti_{0.5}Zr_{0.5}N$	7.70	2.67	1.54	2.25	2.65
$Ti_{0.25}Zr_{0.75}N$	7.79	2.71	1.95		2.68
ZrN	8.63 (7.17-8.02) ^{a,b}	2.86	1.09	2.60	3.26 (3.6) ^d
Au	8.76 (8.9) ^e	4.12	5.49	1.65 (2.3) ^e	4.11

^aFrom Phys. Scr. 25, 775 (1982); ^bFrom Adv. Mat. 25, 3264 (2013); ^cFrom Phys. Rev. B 30, 1155 (1984);

^dFrom Phys. Rev. B 31, 1244 (1985) ; ^eFrom Laser Photon. Rev. 4, 795-808 (2010)

4. Discussion

Here we discuss the performances of TiN, ZrN and their alloys $Ti_xZr_{1-x}N$ with Au and Ag in terms of various quality factors. To visualize the performance of these materials for different classes of plasmonic devices, we apply two quality factors defined for localized surface plasmon resonance (LSPR) and surface plasmon polariton (SPP). LSPR and SPP systems support localized and propagating plasmonic oscillations at the surface of metallic components and their quality factors, Q_{LSPR} and Q_{SPP} , can be expressed in terms of their dielectric functional formulism as shown in Eqs. (5) and (6), respectively [5],

$$Q_{LSPR} = \frac{\omega \frac{d\varepsilon_1(\omega)}{d\omega}}{2\varepsilon_2(\omega)}, \quad (5)$$

$$Q_{SPP} = \frac{\varepsilon_1(\omega)^2}{\varepsilon_2(\omega)}, \quad (6)$$

Calculated Q_{LSPR} and Q_{SPP} are shown in Figs. 5(a) and 5(b), respectively, along with those of Au and Ag for comparison. As seen from above figures, Ag outperforms other materials in the whole visible spectrum. ZrN is the second best material followed by Au. Considering the chemical stability and cost of ZrN, the results suggest that ZrN is a practically appealing for LSPR and SPP applications in visible range which include plasmon-assisted bio-imaging, surface enhanced Raman scattering and plasmonic waveguides. Among the applications of surface plasmon, the LSPRs excited at plasmonic nanostructures have found applications which utilize both scattering and absorption properties.

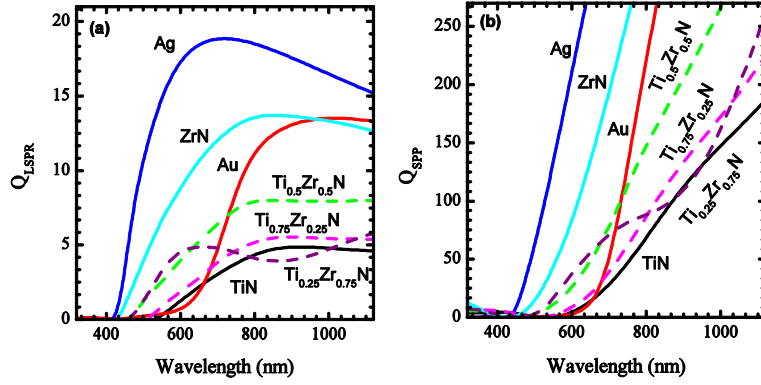


Fig.5 Comparison of (a) Q_{LSPR} and (b) Q_{SPP} of $Ti_{1-x}Zr_xN$ alloy system with those of Au (red line) and Ag (blue line).

To study the LSPRs of $Ti_{1-x}Zr_xN$ alloy system, a simple case where a nanosphere embedded in an isotropic homogenous host material is considered and the scattering (Q_{sca}) and absorption (Q_{abs}) efficiencies are calculated by using the numerical solution of Mie theory [38]. Using the DFT calculated bulk dielectric functions shown in Fig. 4(a) and 4(b) and taking the radius and host index of 30 nm and 1.33, respectively, we plotted the Q_{sca} and Q_{abs} efficiencies of $Ti_{1-x}Zr_xN$ alloy system along with those of Au and Ag as shown in Figs. 6(a) and 6(b). One can notice that barring Ag, ZrN has the highest Q_{sca} value of 2.2 at 488 nm (2.54 eV). On the other hand, TiN has broader resonance with a maximum Q_{sca} value of 0.28 at 603 nm (2.06 eV). Almost similar behavior is observed for the absorption efficiency of these materials as ZrN with a value of 4.71 at a wavelength of 482 nm (2.57 eV) shows the highest efficiency in the alloy system, which is comparable to that of Ag. On the other hand TiN shows much broader resonance similar to Au.

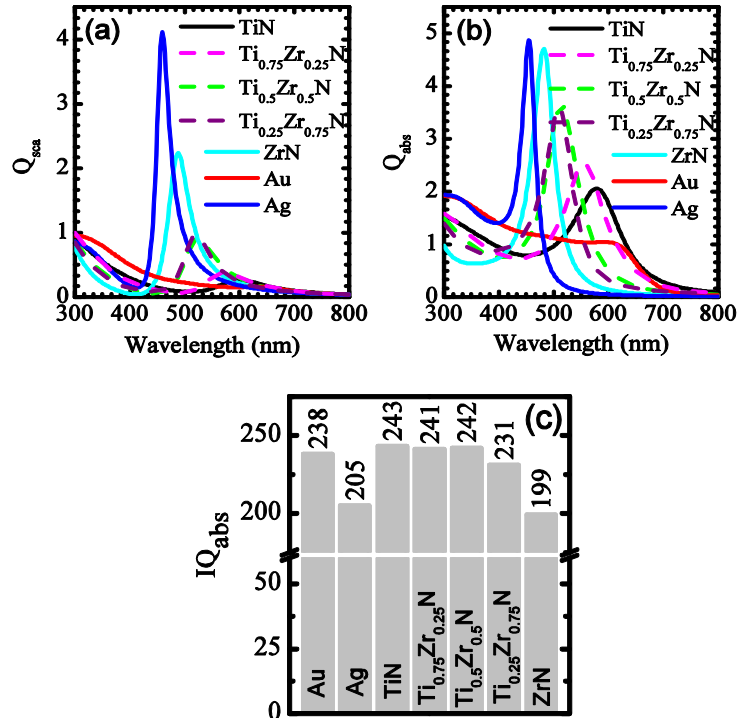


Fig.6 Comparison of (a) scattering, (b) absorption and (c) integrated absorption efficiencies of $Ti_{1-x}Zr_xN$ alloy system with those of Au and Ag.

While the value of Q_{abs} is important at single wavelength illumination, the integrated absorption efficiency is a figure of merit for broadband absorption. With this regard, we calculate the integral of Q_{abs} (IQ_{abs}) at 300-1300 nm, which is the transparent region of water, and plotted in Fig. 6(c). It is observed that IQ_{abs} of TiN and $\text{Ti}_{1-x}\text{Zr}_x\text{N}$ ($x \geq 0.5$) are higher than that of Au. This comparison shows that TiN and the alloy nanoparticles can be good sunlight absorbers in the form of nanofluids [39].

5. Conclusion

Ternary plasmonic compound $\text{Ti}_{1-x}\text{Zr}_x\text{N}$ was studied to examine the correlation between electronic band structure and optical properties, as well as the tunability of plasmonic properties through the band engineering. Our detailed investigation based on first-principles DFT calculations and electromagnetic simulations (Mie theory) revealed that $\text{Ti}_{1-x}\text{Zr}_x\text{N}$ alloy system possess a great potential to be used as tunable plasmonic materials with their highly metallic properties as well as low optical losses. Among the $\text{Ti}_{1-x}\text{Zr}_x\text{N}$ alloys, ZrN is found to be the best low-loss material whereas TiN has higher loss than ZrN. This was due to the low threshold onset of interband energy (1.95 eV) than ZrN where threshold energy for onset of interband transitions is higher (2.60 eV). Due to isostructural nature of these alloy systems, a monotonic behaviors in electronic and optical properties were observed with cation alloying. Such monotonic property is beneficial if one wants to find a plasmonic material with a specific cross-over wavelength. We believe that the alloy system of $\text{Ti}_{1-x}\text{Zr}_x\text{N}$ further broaden the choices of alternative plasmonic materials.

Acknowledgments

This work was partly supported by the Core Research for Evolutional Science and Technology (CREST) program, funded by the Japan Science and Technology Agency (JST).

References

1. J. L. West and N. J. Halas, "Engineered nanomaterials for biophotonics applications: Improving sensing, imaging, and therapeutics," in *Annu. Rev. Biomed Eng.* **5**(1), 285-292 (2003).
2. H. A. Atwater and A. Polman, "Plasmonics for improved photovoltaic devices," *Nat. Mater.* **9**(3), 205-213 (2010).
3. M. Hochberg, T. Baehr-Jones, C. Walker, and A. Scherer, "Integrated plasmon and dielectric waveguides," *Opt. Express* **12**(22), 5481-5486 (2004).
4. A. V. Kildishev and V. M. Shalaev, "Engineering space for light via transformation optics," *Opt. Lett.* **33**, 43-45 (2008).
5. P. R. West, S. Ishii, G. V. Naik, N. K. Emani, V. M. Shalaev, and A. Boltasseva, "Searching for better plasmonic materials," *Laser Photon. Rev.* **4**, 795-808 (2010).
6. G. V. Naik, V. M. Shalaev, and A. Boltasseva, "Alternative Plasmonic Materials: Beyond Gold and Silver," *Adv. Mater.* **25**, 3264-3294 (2013).
7. V. Amendola, R. Saija, O. M. Marago, and M. A. Iati, "Superior plasmon absorption in iron-doped gold nanoparticles," *Nanoscale* **7**, 8782-8792 (2015).
8. J. Suntivich, Z. Xu, C. E. Carlton, J. Kim, B. Han, S. W. Lee, N. Bonnet, N. Marzari, L. F. Allard, H. A. Gasteiger, K. Hamad-Schifferli, and Y. Shao-Horn, "Surface composition tuning of Au-Pt bimetallic nanoparticles for enhanced carbon monoxide and methanol electro-oxidation," *J. Am. Chem. Soc.* **135**, 7985-7991 (2013).
9. M. W. Knight, L. Liu, Y. Wang, L. Brown, S. Mukherjee, N. S. King, H. O. Everitt, P. Nordlander, and N. J. Halas, "Aluminum plasmonic nanoantennas," *Nano. Lett.* **12**, 6000-6004 (2012).
10. M. G. Blaber, M. D. Arnold, and M. J. Ford, "Designing materials for plasmonic systems: the alkali-noble intermetallics," *J. Phys. Condens. Matter* **22**, 095501 (2010).
11. U. Guler, A. Boltasseva, and V. M. Shalaev, "Refractory Plasmonics," *Science* **344**, 263-264 (2014).
12. G. V. Naik, J. Kim, and A. Boltasseva, "Oxides and nitrides as alternative plasmonic materials in the optical range," *Opt. Mat. Express* **1**, 1090-1099 (2011).
13. U. Guler, G. V. Naik, A. Boltasseva, V. M. Shalaev, and A. V. Kildishev, "Performance analysis of nitride alternative plasmonic materials for localized surface plasmon applications," *Appl. Phys. B: Lasers Opt.* **107**, 285-291 (2012).
14. G. V. Naik, J. L. Schroeder, X. Ni, A. V. Kildishev, T. D. Sands, and A. Boltasseva, "Titanium nitride as a plasmonic material for visible and near-infrared wavelengths," *Opt. Mat. Express* **2**, 478-489 (2012).
15. P. Carvalho, F. Vaz, L. Rebouta, L. Cunha, C. J. Tavares, C. Moura, E. Alves, A. Cavaleiro, P. Goudeau, E. Le Bourhis, J. P. Riviere, J. F. Pierson, and O. Banakh, "Structural, electrical, optical, and mechanical characterizations of decorative ZrOxNy thin films," *J. Appl. Phys.* **98**, 023715 (2005).

16. J. M. Chappé, F. Vaz, L. Cunha, C. Moura, M. C. Marco de Lucas, L. Imhoff, S. Bourgeois, and J. F. Pierson, "Development of dark Ti(C,O,N) coatings prepared by reactive sputtering," *Surf. Coat. Technol.* **203**, 804-807 (2008).
 17. G. Onida, W.G. Schmidt, O. Pulci, M. Palummo, A. Marini, C. Hogan, and, R. Del Sole, "Theory for modeling the optical properties of surfaces," *Phys. Status Solidi (a)* **188** 1233-1242 (2001).
 18. G. Onida, L. Reining, and A. Rubio, "Electronic excitations: Density-functional versus many-body Green's-function approaches," *Rev. Mod. Phys.* **74** 601-659 (2002).
 19. K. Glantschnig and C. Ambrosch-Draxl, "Relativistic effects on the linear optical properties of Au, Pt, Pb and W," *New J. Phys.* **12**, 103048 (2010).
 20. M. G. Blaber, M. D. Arnold, and M. J. Ford, "Optical properties of intermetallic compounds from first principles calculations: a search for the ideal plasmonic material," *J. Phys. Condens. Matter* **21**, 144211 (2009).
 21. J. Kim, G. V. Naik, A. V. Gavrilenko, K. Dondapati, V. I. Gavrilenko, S. M. Prokes, O. J. Glembocki, V. M. Shalaev, and A. Boltasseva, "Optical Properties of Gallium-Doped Zinc Oxide—A Low-Loss Plasmonic Material: First-Principles Theory and Experiment," *Phys. Rev. X* **3**, 041037 (2013).
 22. A. Calzolari, A. Ruini, and A. Catellani, "Transparent Conductive Oxides as Near-IR Plasmonic Materials: The Case of Al-Doped ZnO Derivatives," *ACS Photonics* **1**, 703-709 (2014).
 23. S. Laref, J. Cao, A. Asaduzzaman, K. Runge, P. Deymier, R. W. Ziolkowski, M. Miyawaki, and K. Muralidharan, "Size-dependent permittivity and intrinsic optical anisotropy of nanometric gold thin films: A density functional theory study," *Opt. Express* **21**, 11827-11838 (2013).
 24. J. Kim, S.-H. Jhi, and K. Ryeol Lee, "Color of TiN and ZrN from first-principles calculations," *J. Appl. Phys.* **110**, 083501 (2011).
 25. G. D. Mahan, *Many-Particle Physics*, (Springer, 2000).
 26. M. Gajdoš, K. Hummer, G. Kresse, J. Furthmüller, and F. Bechstedt, "Linear optical properties in the PAW methodology," *Phys. Rev. B* **73**(4) 045112 (2006).
 27. M. Kumar, H. Zhao, and C. Persson, "Study of band-structure, optical properties and native defects in A(DB(III)O(2) (A(I) = Cu or Ag, B-III = Al, Ga or In) delafossites," *Semicond. Sci. Technol.* **28**, 065003 (2013).
 28. M. Kumar, N. Umezawa, and M. Imai, "(Sr,Ba)(Si,Ge)₂ for thin-film solar-cell applications: First-principles study," *J. Appl. Phys.* **115**, 203718 (2014).
 29. G. Kresse and J. Furthmüller, "Efficient iterative schemes for ab initio total-energy calculations using a plane-wave basis set," *Phys. Rev. B Condens. Matter* **54**(16) 11169-11186 (1996).
 30. J. P. Perdew, K. Burke, and M. Ernzerhof, "Generalized gradient approximation made simple," *Phys. Rev. Lett.* **77**, 3865-3868 (1996).
 31. V.J. Keast, B. Zwan, S. Supansomboon, M.B. Cortie, P.O.Å. Persson, "AuAl₂ and PtAl₂ as potential plasmonic materials," *J. Alloys Comp.* **577**, 581-586 (2013).
 32. S. Gražulis, D. Chateigner, R. T. Downs, A. F. T. Yokochi, M. Quirós, L. Lutterotti, E. Manakova, J. Butkus, P. Moeck, and A. Le Bail, "Crystallography Open Database – an open-access collection of crystal structures," *J. Appl. Crystallography* **42**, 726-729 (2009).
 33. R. L. Olmon, B. Slovick, T. W. Johnson, D. Shelton, S.-H. Oh, G. D. Boreman, and M. B. Raschke, "Optical dielectric function of gold," *Phys. Rev. B* **86**, 235147 (2012).
 34. B. Karlsson, R. P. Shimshock, B. O. Seraphin, and J. C. Haygarth, "Optical Properties of CVD-Coated TiN, ZrN and HfN," *Phys. Scr.* **25**, 775 (1982).
 35. P. Prieto, F. Yubero, E. Elizalde, and J. M. Sanz, "Dielectric properties of Zr, ZrN, Zr₃N₄, and ZrO₂ determined by quantitative analysis of electron energy loss spectra," *J. Vac. Sci. Technol. A* **14**(6), 3181 (1996).
 36. J. Pflüger, J. Fink, W. Weber, K. P. Bohnen, and G. Crecelius, "Dielectric properties of TiCx, TiNx, VCx, and VNx from 1.5 to 40 eV determined by electron-energy-loss spectroscopy," *Phys. Rev. B* **30**, 1155-1163 (1984).
 37. J. Pflüger, J. Fink, W. Weber, K. P. Bohnen, and G. Crecelius, "Dielectric properties of ZrN, NbC, and NbN as determined by electron-energy-loss spectroscopy," *Phys. Rev. B* **31**, 1244-1247 (1985).
 38. C. F. Bohren and D. R. Huffman, *Absorption and Scattering of Light by Small Particles* (Wiley, 2008).
 39. S. Ishii, R. P. Sugavaneshwar, K. Chen, T. D. Dao, and T. Nagao, "Sunlight absorbing titanium nitride nanoparticles," *ICTON 2015 proceeding*, DOI:10.1109/ICTON.2015.7193490.
-